This is the accepted manuscript made available via CHORUS. The article has been published as:

Interface between Sr_{2}RuO_{4} and Ru-metal inclusion: Implications for its superconductivity

Soham S. Ghosh, Yan Xin, Zhiqiang Mao, and Efstratios Manousakis

Phys. Rev. B **96**, 184506 — Published 8 November 2017

DOI: 10.1103/PhysRevB.96.184506

The interface between Sr_2RuO_4 and Ru-metal inclusion–Implications for its superconductivity

Soham S. Ghosh[1,2], Yan Xin[2], Zhiqiang Mao[3], and Efstratios Manousakis[1,2,4]
[1] *Department of Physics, Florida State University, Tallahassee, Florida 32306-4350, USA*
[2] *National High Magnetic Field Laboratory, Florida State University, Tallahassee, Florida 32306-4350, USA*
[3] *Department of Physics, 5024 Percival Stern Hall, Tulane University, New Orleans, LA 70118 USA*
[4] *Department of Physics, University of Athens, Panepistimioupolis, Zografos, 157 84 Athens, Greece*
(Dated: October 25, 2017)

Under various conditions of the growth process, when the presumably unconventional superconductor Sr_2RuO_4 (SRO) contains micro-inclusions of Ru metal, the superconducting critical temperature increases significantly. An atomic resolution high-angle-annular-dark-field (HAADF) scanning transmission electron microscopy (STEM) study shows a sharp interface geometry which allows crystals of SRO and of Ru-metal to grow side by side by forming a commensurate superlattice structure at the interface. In an attempt to shed light as to why this happens, we investigated the atomic structure and electronic properties of the interface between the oxide and the metal micro-inclusions using density functional theory (DFT) calculations. Our results support the observed structure indicating that it is energetically favored over other types of Ru-metal/SRO interfaces. We find that a t_{2g}-e_g orbital mixing occurs at the interface with significantly enhanced magnetic moments. Based on our findings, we argue that an inclusion mediated interlayer coupling reduces phase fluctuations of the superconducting order parameter which could explain the observed enhancement of the superconducting critical temperature in SRO samples containing micro-inclusions.

I. INTRODUCTION

The superconducting state of Sr_2RuO_4 (SRO) has been intensively studied[1] since its discovery in 1994[2]. SRO is a layered perovskite oxide sharing the same structure as La_2CuO_4, one of the parent compounds of the cuprate superconductors, and it is believed to be a p-wave superconductor with odd spin-triplet pairing.[1,3–8] A chiral orbital order parameter of the form $p_x + ip_y$ has been suggested by time-reversal symmetry breaking experiments[9,10]. The role of strong ferromagnetic spin fluctuations in mediating superconductivity has been pointed out[11]. Theoretical[12,13] and experimental investigations which were carried out before 2002 have been reviewed[1]. Quantum oscillation experiments[14] indicate that the normal state can be understood as a two dimensional Fermi liquid[1].

The electronic properties have been studied by a number of methods which are summarized in Ref. 1, including the local density approximation (LDA) method[15,16] and the generalized gradient approximation (GGA)[17,18] method. Depending on the exchange correlation functional used, GGA predicts either a nonmagnetic state[18] or a antiferromagnetic (AF) state[17] with ferromagnetically ordered RuO_2 basal planes. There is evidence for incommensurate antiferromagnetic spin fluctuations[19,20] and it has been shown that ferromagnetic and antiferromagnetic fluctuations co-exist in this oxide.[21].

In more recent studies, superconductivity in bulk SRO is found to be enhanced under uniaxial $\langle 001 \rangle$[22], $\langle 100 \rangle$ and $\langle 110 \rangle$ strains where in the latter two cases strain-driven asymmetry of the lattice is believed to cause a change in symmetry of the superconducting order parameter[23]. T_c is also found to be enhanced due to dislocations[24], and in a system where there is an interface of W/Sr_2RuO_4 point contacts[25].

The unexpected enhancement of T_c from 1.5 K to almost 3 K, when micro-sized ruthenium metal inclusions are embedded inside SRO in the eutectic system during crystal growth[26], is a very interesting and unexplained phenomenon. There is evidence[27] that the "3-K" superconducting phase is unconventional with the presence of a hysteresis loop[28]. In this "3-K" phase, the ruthenium micro-platelets are not uniquely oriented with respect to the SRO lattice. This, together with large diamagnetic shielding could suggest the existence of interface superconductivity at the Ru-SRO interface, residing primarily in SRO[26]. Sigrist and Monien's[29] phenomenological analysis postulates a superconducting state with different symmetry and higher T_c than in the bulk.

HAADF-STEM images of a representative interface were presented in Ref. 30 and in the present paper with higher resolution as shown in Fig. 1. Here, we explore the atomic structure, stability and the electronic properties of this interface using density functional theory (DFT) calculations. We notice that this stable interface is perpendicular to the SRO bulk crystallographic a axis and has alternating intact meandering Ru-O octahedra, which can be conceived as continuations of the bulk SRO RuO_2 planes. Alternating pairs of Ru columns (which, as we show, are coordinated by oxygen atoms which are not visible in the HAADF-STEM images) fill in the gaps created by the meandering interface at the same periodicity as the SRO unit cell along the crystallographic c axis. We show that these pair columns of Ru atoms have a coordination number different from that in the metal phase and that in the SRO phase. A nearly perfect hcp crystal of Ru metal grows from the next metal layer with a small lattice mismatch that eventually relaxes as one moves away from the interface and into the inclusion.

In the lowest energy interface the Ru-metal grows its first layer commensurate with the SRO interface at a wavelength which nearly corresponds to eleven Ru metal atoms for every two periods of the SRO crystal along its own c axis. Therefore, the inclusions connect RuO_2 planes through a commensurate interface which is almost perfectly ordered at the atomic scale.

We show that this interface is stable against phase separation and it is more stable than other conceivable interfaces between SRO and Ru-metal. A spin polarized GGA calculation yields significant magnetic moments of the Ru atoms in the SRO phase near the interface. Our study establishes a clear picture of the stable Ru-Sr_2RuO_4 interface which is important in understanding the unconventional "3-K" phase.

We also argue that our findings, that the Ru inclusions form a nearly atomically perfect interface with the SRO crystal, imply the emergence of a significant interlayer coupling which could give rise to reduction of phase fluctuations of the superconducting order parameter characterizing the various RuO_2 planes. This is expected to lead to an enhancement of the superconducting critical temperature as observed in the SRO crystals with Ru inclusions.

The paper is structured as follows. In Sec. II, we present our experimental results and the computational details of our DFT calculations of the observed interface structure and stability consideration of various terminations. In Sec. III, we analyze the experimentally observed interface in the light of the DFT-based calculations and also discuss our detailed results obtained from these calculations. In Sec. IV, we discuss the possible causes of increased T_c based on our findings. Last, in Sec. V, we highlight our conclusions and the implications of this work.

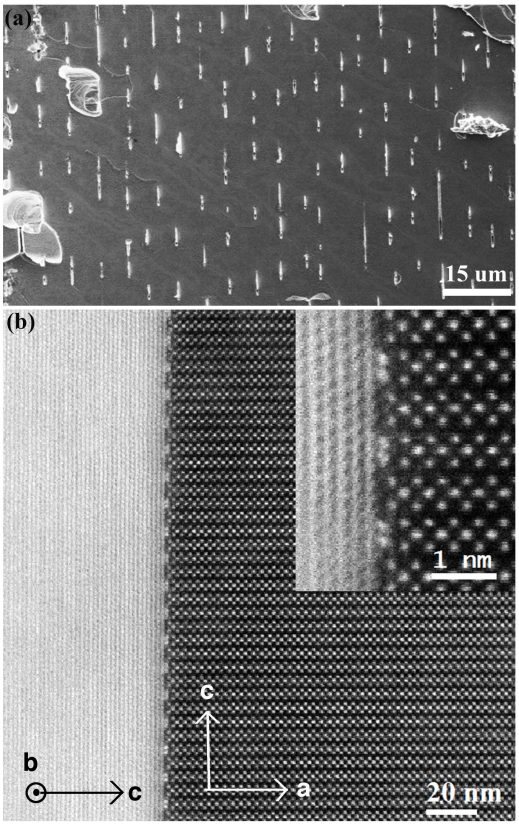

FIG. 1. (a) Scanning electron microscope image of a cleaved (001) Sr_2RuO_4 bulk crystal containing parallel Ru micro-platelets (brighter contrasted short lines). (b) HAADF-STEM image of the Sr_2RuO_4/Ru interface at lower magnification showing an atomically straight and sharp super-structured interface, where the brighter region on the left is the Ru metallic inclusion and on the right is the Sr_2RuO_4 phase. The brightest spots are Ru followed by Sr. O atoms are too faint to be observed. There is no concentration gradient of SRO or Ru on either side of the interface. (inset) Close up view of the interface at higher magnification, where the atomic structure is clearly revealed. The HAADF-STEM images were taken with a probe of 0.078 nm and a convergence semi-angle of 21 mrad and inner collection angle of 78 mrad. Brighter-contrast atoms are Ru atoms while Sr atoms are less bright.

II. EXPERIMENTAL AND DFT STUDY OF THE INTERFACE STRUCTURE

The platelet inclusions are the result of excess Ru (more RuO_2 in the mixture than needed to make stoichiometric SRO) in the initial mixture. We will show by means of DFT calculations that the interface seen in our HAADF-STEM images is low enough in energy to be preferable than macroscopic phase separation of SRO and Ru metal inclusions. In addition, we will show that other related interfaces are energetically higher than the one shown in Fig. 1.

Sr_2RuO_4 occurs in bulk in the body-centered tetragonal structure like the high temperature superconductor La_2CuO_4[31]. Ru, the brightest atoms in the HAADF-STEM images in the SRO phase, and the planar O(1) atoms form a two-dimensional square lattice with Ru-O bond length being 1.95 Å which is less than the sum of the ionic radii of Ru^{4+} and O^{2-}, suggesting planar hybridization[16]. The apical O(2) height above and below is larger at 2.06 Å.

A. Analysis of the observed interface

First, we notice in Fig. 1 and in Fig. 1 of Ref. 30 that the interface is perpendicular to the bulk [100] SRO direction and is terminated at alternating intact meandering Ru-O octahedra, which are continuations of the bulk SRO RuO_2 planes, and alternating pairs of Ru columns filling in the gaps created by the meandering interface. Notice that, as seen in Fig. 1, the Ru ions of the metallic interface, without any significant change of the unit-cell size, form an interface at a commensurate wavelength nearly twice that of the SRO unit-cell size in the [001] direction (corresponding to eleven

unit cells of pure Ru crystal). The commensurate growth leaves a small lattice mismatch between the SRO layers near the interface and those deeper in the bulk. This causes a strain that grows with system size until it becomes energetically favorable to produce dislocations[24] relieving the strain. As seen in the transmission electron microscopy (TEM) images in Ref. 24, the dislocations are complex structures which occur, for a sharp and flat interface, over a length scale longer than that visible in Fig. 1. These structures are beyond the scope of our present *ab initio* calculations and we focus here on the microscopic length scale at which the interface is free of dislocations.

To verify that the interface columns are Ru atoms, in Table I we provide the average HAADF-STEM intensity of several atomic columns (along the SRO [010] direction), as well as the electron energy loss spectroscopy (EELS) measured sample thickness at those column locations. The TEM sample preparation of such a hetero-structural interface creates sudden thickness change within a few nm at the interface between two such dissimilar materials that have a different milling rate. The atomic column intensity in the HAADF-STEM image scales proportionally with sample thickness and is affected by crystal orientation. As we shall see in subsequent sections, the average nearest neighbor distance along the beam direction for the interface Ru pair atoms is 3.9 Å, the same as that in SRO. The intensity is marginally higher for the interface Ru atoms because the interface columns are slightly thicker than the SRO bulk region (see Table I). In addition, there is higher background noise at the interface due to contamination and scattering from adjacent Ru atoms in the Ru platelet. Given that the columns in the hcp platelet have more Ru atoms than those in the SRO phase and those in the interface columns, we find the column intensity in the hcp platelet to be somewhat lower than expected. This is due to the fact that the intensity of the Ru atoms in the platelet is more diffused than in SRO, as can be clearly seen from Fig. 1. Here the Ru atom columns are not lined up precisely along the beam direction and therefore the dynamical scattering effect is less in the platelet. We confirmed this by changing the window size of intensity measurement and we find that the largest change is in the intensity of the platelet columns. The small misalignment angle ($< 1^\circ$), over a column several hundred atoms thick, is enough to reduce the intensity noticeably. It is, however, too small to be taken into account in our DFT calculations. Namely, to take such a small misalignment into account it would require a unit cell containing several tens of times more atoms than the unit cell presently used. Therefore, we have assumed perfect alignment between the SRO and the hcp phase in this direction in our computational work as we do not expect such a small deviation from the perfect alignment to yield a significant effect.

Atom	Sr	Ru	Ru	Ru	Ru
Location	SRO	SRO	interface	1^{st} hcp layer	3^{rd} hcp layer
Intensity (10^{23} e)	3.78	4.26	4.90	5.05	5.33
Error ($\pm$)	0.10	0.10	0.08	0.08	0.08
Thickness (nm)	43.2	43.2	47.09	47.09	49.63
Error ($\pm$)	0.54	0.54	0.91	0.91	0.68

TABLE I. The average atomic column intensity and EELS – measured sample thickness in respectively the SRO phase, in the interface pair columns, in the first hcp layer (closest to the interface) and in the third hcp layer. The intensity is calculated as the sum of pixel intensity of one atom column within a window of 15×17 pixel size in units of 10^{23} electrons.

HAADF-STEM image provides direct information on the interface structure but leaves an ambiguity on any oxygen atom near the interface and the Ru atom positions in the SRO [010] direction which is perpendicular to the HAADF-STEM field of view. This is the first item to address by means of our DFT calculations, the technical details of which are discussed later. By examining various possibilities, we find that in their optimum positions, the Ru pair columns bridge diagonal oxygen atoms of the terminating SRO layer. On one side of the interface these Ru pair columns form a similar type bond to oxygen atoms as the 1.95 Å Ru-O bond in the rutile phase of RuO_2, and on the other side they have an hcp Ru metal environment. This arrangement leaves the meandering SRO termination layer unchanged subject to ionic relaxations, and is consistent with the experimental image in Fig. 1. Therefore, we believe that this part of our DFT study complements the HAADF-STEM image and we now have a complete picture of the structure of the interface.

B. Stability of the interface

The implementation of the observed structure by DFT calculation ideally requires at least eleven bulk unit cells of the hcp Ru metal phase commensurate with two conventional bulk unit cells of the SRO along the SRO [001] axis, and at least six bulk unit cells of the hcp Ru commensurate with four bulk units cells of the SRO along the SRO [010]

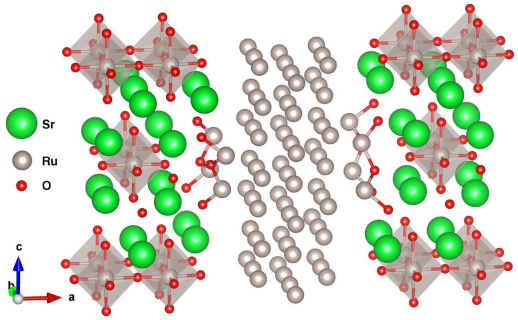

FIG. 2. (color-online) Sr_2RuO_4-Ru supercell used for spin-GGA calculations of the heterojunction as generated by VESTA software package. There are three different Ru-O bond lengths: The Ru-O bond lengths in the interface columns are the shortest, followed by the in-plane Ru-O(1) distances, followed by the Ru-O(2) bond lengths. The interface Ru atoms columns mediate between the SRO phase and the Ru metallic phase. We show part of the next repeated image for clarity. SRO lattice vectors are shown.

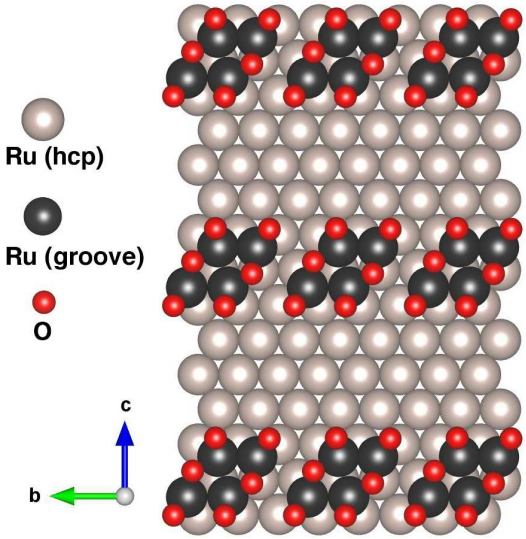

FIG. 3. (color-online) The SRO $b-c$ plane showing the two layers of the SRO-Ru interface, formed by the interface Ru pair columns and the terminating layer of the hcp metal. The unit cell lengths are slightly different from ideal bulk values (with details in the text). The triangular lattice of the Ru metal layer and the rectangular lattice of the interface Ru pairs are commensurate with 7.81 Å $\times$13.52 Å wavelengths in the SRO [010] and [001] directions respectively. The Ru columns are situated in the low energy valleys of the triangular lattice. The experimental wavelength is at least twice in each direction with an increased fraction of misalignment where some interface columns are located away from the hcp valleys, but the idea of commensuration between a rectangular and a triangular lattice is preserved.

direction. Such a supercell proved computationally unfeasible, particularly due to the large number of ruthenium atoms. Instead, to keep the supercell size reasonable, we used a supercell geometry with a stretched unit cell length of 13.52 Å along the SRO [001] direction and double the SRO bulk unit cell length in the SRO [010] direction.

In this reduced supercell containing 128 atoms, shown in Fig. 2, one conventional bulk SRO unit cell is commensurate with six bulk hcp Ru unit cells along SRO [001] and two bulk SRO unit cells are commensurate with three bulk metal unit cells in the SRO [010] direction. The atoms have been relaxed to their final positions. This geometry stretches the SRO c-axis by 5 % and compresses the a, b axes of the hcp Ru by 4 % each. The apical O(2) height is increased

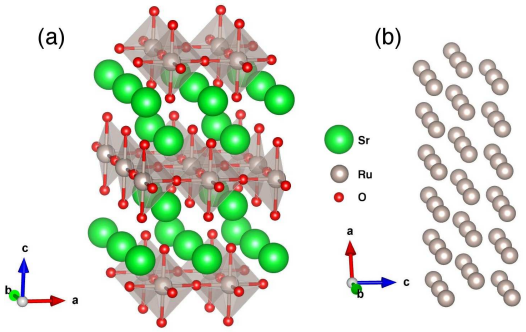

FIG. 4. (color-online) (a) The 2.5-layer thick Sr_2RuO_4 slab with equivalent (010) surfaces used to compute the energy of (001) linear strain changing the c-lattice vector length from 12.9 Å to 13.52 Å while keeping the a and b-vectors same as in bulk. (b) The 1.5-layer thick ruthenium metal slabs in its hcp structure with (001) surfaces used to compute the energy of planar compression. The a, b lattice vectors were each reduced from 2.73 Å to 2.61 Å. In both calculations we used at least 15 Å of vacuum between repeated images.

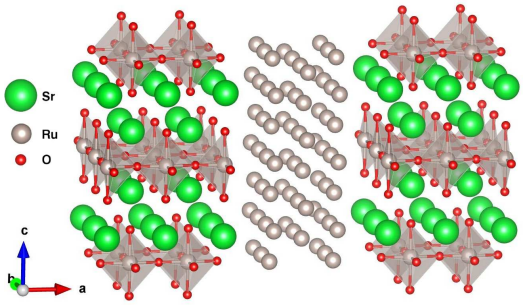

FIG. 5. (color-online) A hypothetical interface between SRO [100] and Ru hcp [001] surfaces, created from the slabs in Fig. 4 by bringing them together gradually and allowing the atoms to relax till the optimum interlayer distance at the interface is reached. This geometry is similar to that in Fig. 2 except in the absence of the Ru interface columns. The hcp c-axis is parallel to the SRO [100] direction. Part of the next repeated image is shown for clarity.

from 2.06 Å to 2.09 Å. In Fig. 3 we show the SRO $b-c$ plane of the two layers of the SRO-Ru interface formed by the interface Ru pair columns and the terminating layer of the hcp metal. Even though we will use this smaller super-cell in our DFT implementation, by carrying out various types of optimization calculations it will become reasonably clear that the observed structure is indeed the most energetically favorable among various other plausible atomic configurations.

Table II summarizes our stability analysis results. We describe the procedure and the notations below.

First, we find that the energy needed for breaking apart the interface of our reduced structure to create the two constituent slabs - SRO with [100] surfaces and Ru metal with [001] surfaces (Fig. 4 and denoted by "slabs" in Table II) - to be 13.16 eV, a significant amount of energy.

Second, we compare the energy of our reduced structure to the energy of a similar supercell but with flat SRO [100] - Ru [001] interface (shown in Fig. 5 and denoted by "flat" in Table II) which we compute by bringing the SRO and Ru phases closer in small steps and relaxing the ions around their positions to find the minimum of the energy. We find that this supercell is higher in energy by 8.37 eV compared to our reduced meandering geometry in Fig. 2. Thus the meandering octahedra and the interface ruthenium columns are necessary to stabilize the interface. In both the above calculations, there are 128 atoms on either side of the equation and we account for the balance of atoms in the non-meandering structures by putting the extra Ru pair columns of the interface in a ruthenium bulk phase, which is the most stable ruthenium phase. To describe why the meandering Ru interface columns are necessary, consider

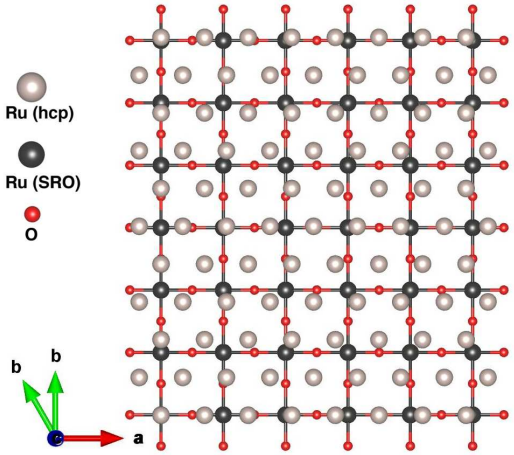

FIG. 6. (color-online) A possible interface between (001) SRO and hcp Ru metal with a 19.52 Å ×23.42 Å superlattice where after a 0.8 % strain on the hcp plane, five planar unit cells of RuO_2 is commensurate with seven unit cells of the Ru metal in the SRO [100] direction and six unit cells of RuO_2 is commensurate with five unit cells of the Ru metal in the SRO [010] direction. Most of the atoms at the interface are frustrated and experience the laterally averaged potential leading to very little energy gain. Both SRO and Ru-metal lattice vectors are shown.

the two interface layers ($b-c$ plane of SRO) in Fig. 3. We note that the interface Ru columns form a rectangular planar lattice (which is commensurate with the same periodicity of our reduced interface geometry) adjacent to the triangular lattice of the terminating Ru metal plane. Furthermore, the interface Ru pairs to a large extent are situated in potential valleys where the atoms of the next Ru hcp layer would have been in absence of an interface.

Third, having established the necessity of the meanders, we argue that the larger interface with eleven unit cells of Ru-metal in the SRO [001] direction and six Ru-metal unit cells in the SRO [010] direction is more stable than our computed reduced interface as follows.

The reduced geometry suffers from artificial planar compression of its Ru metal phase and uniaxial strain of its SRO phase but it accommodates the interface Ru pair columns in the grooves created by the terminating hcp Ru layer. By sliding the Ru metal phase across the interface in Fig. 2, we find that this is indeed an energy minimum. The larger experimentally observed periodicity breaks this symmetry and at least some of the Ru column pairs are misaligned with respect to the hcp layer. This leads to frustration in the terminating hcp layer of the metal, as can be observed directly in Fig. 1. To a first approximation, the price of lattice length manipulation can be calculated by computing the sum of the individual energy losses caused by separately compressing an ideal Ru metal slab and stretching an ideal SRO slab (Fig. 4) to their respective values necessary to create the reduced supercell shown in Fig. 2. We find this energy to be 8.54 eV. On the other hand, the energy loss due to non alignment of the Ru interface pair columns in the experimentally observed geometry can be upper bounded by sliding the Ru metal layers of the reduced geometry along the interface, thus moving the Ru pair columns away from the potential valleys of the hcp layer, until we reach an energy maximum.

The maximum cost of misalignment of the interface Ru pair columns is 4.49 eV, less than the cost of stretching and compressing the constituent phases. It follows that in any interface between the SRO (100) surface and Ru (001) surface, meandering Ru interface columns with the experimentally observed periodicity is the most stable structure. We denote this configuration in which the SRO slab is compressed and Ru metal is stretched, but as a result the interface will be aligned, as "aligned" in Table II.

As a final part of our stability argument, we consider the possibility that there can be other types of interfaces without these interface Ru columns which are more stable that ours. In particular, the (001) surface of SRO can be cleaved with a terminating SrO or RuO_2 layer and its interface with a ruthenium hcp layer can be conceived. We show in Fig. 6 a commensurate geometry at the interface, in which a 5×6 RuO_2 superstructure (defined along the SRO a and b-axes respectively) is commensurate with a 7×5 superstructure of the metal, after accounting for a 0.8 % uniaxial strain on the Ru metal. Most of the atoms of each phase in this superlattice are randomly oriented with those of the other phase and therefore each layer at the interface will experience the laterally averaged potential of the other layer. This is arguably a small energy gain of the order of a few tens of meV for each SRO formula unit. In fact,

any interface without the periodic meanders observed in our experiment is likely to be disfavored for the same reason. A straightforward GGA computation shows that our reduced structure is lower in energy by 1.72 eV compared to the sum of energies of a Ru metal slab similar to that shown in Fig. 4(b) and the appropriate amount of bulk SRO (the sum is denoted by "bulk" in Table II), a surprising result. The experimentally observed superlattice should be even more stable. We conclude therefore that the observed meandering interface is favored even over phase separation of the eutectic mixture between bulk SRO and Ru. Therefore, we cannot think of any other interface which can compete with the one observed by our HAADF-STEM study.

Lastly, the following question arises. Since we find that the observed interface lowers the energy with respect to bulk SRO and a semi-infinite Ru metal, why the system does not try to create more such interfaces and instead it grows mesoscopic size inclusions. Indeed, our findings indicate that the lowest energy state of such a system of SRO with excess Ru metal should be a state with a high density of such interfaces separated by a microscopic-size length. However, the combined system was created under non-equilibrium conditions of the eutectic mixture which do not allow for the system to search for a global lowest energy state. First, at a relatively short-time scale the free energy is only locally minimized and, then, the system freezes in a macroscopic state of domains which require an overwhelmingly large amount of time to find the state which is the global minimum. More specifically, once a few layers of Ru metal have grown, it becomes locally energetically favorable for more Ru atoms from the excess of Ru, to attach themselves to those existing Ru metal layer. Forming another interface which combines a simultaneous and coherent arrangement of many atoms is a much slower process (i.e., a low entropy state) than simply adding to the existing Ru metal layer an additional single Ru atom. This means that the path to the actual ground state is "narrow" and requires a very slow process and, as a result, the system gets stuck in other metastable local free-energy minima. Thus, although a high density of such interfaces is preferred by taking into consideration just the energy of the system, the meandering termination layer of SRO with intact RuO_2 octahedra and interface Ru columns are long-range phenomena generally suppressed by the large entropy present in the high temperature eutectic mixture.

Configuration	slabs	flat	aligned	bulk
E_{tot} (eV)	3.29	2.09	1.01	0.43

TABLE II. Total energy of various geometries per unit interface area using the conventional unit cell of Sr_2RuO_4 as one unit. E_{tot} is defined relative to the most stable state, namely the interface with meanders. For details about the geometries, please see Sec. II B.

C. Computational details

Spin-GGA computations were performed using plane-wave basis set (cutoff of 540 eV) with the projector augmented wave methodology[32] used to describe the wavefunctions of the electrons as implemented in the VASP package[33–36], using the Perdew-Burke-Ernzerhof (PBE) exchange correlation functional[37]. The $4s$, $4p$, $5s$ electrons of strontium, the $5s$, $4d$, $4p$, $4s$ electrons of ruthenium and the $2s$, $2p$ electrons of oxygen were treated as valence electrons. The Brillouin zone of the 128-atoms supercell with the meandering interface geometry (Fig. 2) and the 124-atoms supercell with flat interfaces (Fig. 5) were sampled with $1 \times 6 \times 4$ k-point grid, and 60 k-points were used to compute the electronic density of states (DOS). Increasing the k-point grid from $1 \times 6 \times 4$ to $1 \times 7 \times 5$ leads to a negligibly small change of the total energy of the meandering interface geometry by 0.04 eV and an increase of the moments of the magnetic ruthenium atoms by 0.08 μ_B. The 70-atoms SRO slab (Fig. 4(a)) is 2.5 layers thick with symmetric 2×1 $b-c$ surfaces. We have used a tetragonal geometry with $b = 3.90$ Å and $c = 12.90$ Å for them, and sampled the Brillouin zone with a $1 \times 8 \times 4$ k-point grid. For the 54 atoms Ru metal slab (Fig. 4(b)) which is 1.5 layers thick with a $6 \times 3 \times 1.5$ structure, we have used an hcp unit cell length of 2.739 Å and sampled the Brillouin zone with $4 \times 8 \times 1$ k-point grid. For both the slabs, we have used a vacuum layer at least 15 Å thick. All the supercells was structurally relaxed while keeping the cell shape and cell volume fixed until the forces were converged to less than 10 meV/Å for each ion.

III. ELECTRONIC PROPERTIES

Our computed geometry (Fig. 2) shows a 1.8° rotation of the RuO_6 octahedron on the RuO_2 planes along with small amounts of buckling. The number of atoms and electrons in the supercell prevent us from sampling the Brillouin zone with enough k-point accuracy to compare various magnetic orderings. Various magnetic ordering differ from each

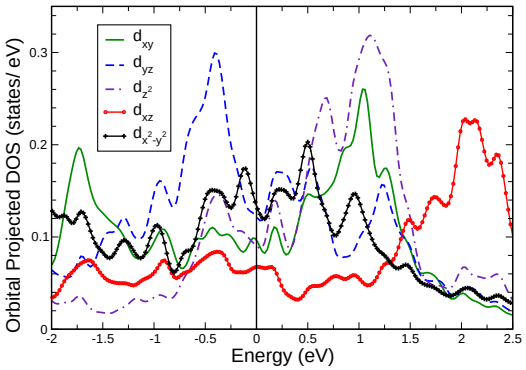

FIG. 7. (color-online) Y_{lm}-projected density of states for a Ru atom from the interface column pair. The atom has a O_2 environment like in the rutile RuO_2 phase with bond angle of 115° and Ru-O bond length of 1.83 Å. On the other hand, it also neighbors the Ru metal closed-pack layer at the interface. Both these environments influence its electronic structure.

other by only a few meV and their accurate study require an extremely dense sampling of k-points[20,38]. Therefore we limit ourselves to the $q = 0$ state, which we find to be lower in energy than the nonmagnetic state. We find no magnetic moments in the interface columns of Ru atoms and metallic phase Ru atoms, but strong magnetic moments in the Ru atoms ($M_{Ru} = 1.532\,\mu_B$) in the SRO phase. GGA calculations have previously predicted[39] surface ferromagnetism in SRO where it was stabilized by a large (9°) surface octahedra rotation and consequent band narrowing. To ensure that this is not purely an effect of the (001) strain, we have performed spin-GGA calculations of bulk SRO with stretched c-axis values. We find in such a system the octahedra rotations are absent and the ground state is ferromagnetic but with much smaller magnetic moments ($M_{Ru} = 0.220\,\mu_B$). Since we consider only translationally invariant $q = 0$ states, the possibility of complex nonzero q states cannot be ruled out. Furthermore, GGA does not correctly account for correlations, so the magnetic picture is to be taken with caution.

In the interface Ru atom columns, there are two different types of RuO_2 bonds in each pair. One has bond angle close to 90° and Ru-O bond length close to the planar Ru-O(1) bond length, whereas the other has bond angle ∼ 115° and Ru-O bond length ∼ 1.83 Å. Both Ru atoms lack the planar square lattice coordination and are expected to have different orbital structure compared to those in SRO. We find the interface Ru atoms in a +3 valence state, consistent with a Bader[40] charge analysis. We also see significant t_{2g}-e_g mixing in each of them. Figure 7 shows the density of states of the Ru atom which has a RuO_2 bond angle of ∼ 115°. Both the $d_{x^2-y^2}$ and d_{z^2} states are pulled down below the Fermi level and mixed with t_{2g} orbitals. $t_{2g} - e_g$ mixing was found at the well-studied $SrTiO_3/LaAlO_3$ interface[41], where an e_g splitting was caused by oxygen vacancy and gave rise to magnetic order. Here, it is caused by severe Ru-O hybridization and non planar RuO_2 geometry.

IV. IMPLICATIONS FOR SUPERCONDUCTIVITY

Superconductivity in Sr_2RuO_4 is believed to arise from pairing within the RuO_2 layers. The interlayer coupling between RuO_2 planes is very weak which is expected to lead to large amplitude phase fluctuations of the order parameter as is the case of the Cuprate superconductivity[42]. These phase fluctuations lower the value of the superconducting transition temperature. In the case where inclusions are present, a remarkably ordered interface geometry between tetragonal unconventional superconductor Sr_2RuO_4 and hexagonal closed pack metal Ru has been discovered as illustrated in both our HAADF-STEM images of Fig. 1 and justified by means of our DFT calculations (Fig. 2) which also reveal the structure along the perpendicular direction as illustrated in our derived highly ordered structure of Fig. 3 (a direction which is hidden from any HAADF-STEM study). These interfaces with a metallic inclusion clearly should lead to an effective interlayer Josephson junction coupling of the superconducting order parameter which reduces these phase fluctuations over. This coupling produced by these ordered inclusions should thus lead to an enhanced T_c as observed in the "3-K" phase. We believe that the reason for the enhancement of T_c due to the inclusions is different from Sigrist and Monien's[29] phenomenological model and from the reason that causes strain driven increase of T_c in pure bulk SRO as seen in Ref. 23. In the latter case the increase is due to the fact that the strain affects the symmetry character (i.e., $p_x + ip_y$) of the superconducting order parameter as argued in Ref. 23.

It has been shown experimentally[26] that inclusions increase the interlayer coherence length and significantly reduce the anisotropy of superconductivity: $\xi_{ab}(0)/\xi_c(0) = 3.6$ in the "3-K" phase with metals inclusions as compared to 20 for the 1.5 K phase SRO.

As discussed in Sec. III, an accurate study of the magnetic ordering of an interface such as ours, with a large number of electrons, is beyond present computational capacity. However, if we take seriously a) our finding, i.e., that the Ru-atom magnetic moments near the interface are increased as compared to bulk, and b) the suggested pairing mechanism due to paramagnon exchange[11], one might not exclude the possibility that the assumption a) leads to an increased electron-paramagnon coupling and as a consequence to a T_c enhancement in the spin-triplet pairing channel. While this scenario is possible, we believe that our observation and calculations discussed in the previous two paragraphs are more likely to be the cause of the enhancement of T_c due to the inclusions.

V. CONCLUSIONS AND IMPLICATIONS

A remarkably ordered interface geometry between tetragonal unconventional superconductor Sr_2RuO_4 and hexagonal closed pack metal Ru formed as metallic inclusions during the growth process of the superconductor has been revealed by HAADF-STEM studies and has been investigated and understood in the present paper using DFT. The heterojunction is characterized by regular columns of Ru pairs in the SRO [001] direction and clean octahedra terminations of the ruthenate oxide. Using DFT, we have correctly reproduced the experimental structure including the positions of interface oxygen atoms and along directions hidden to any HAADF-STEM study and investigated the electronic structure of the interface. We have found rotated octahedra, modified Ru d-orbitals and enhanced magnetic moments near the interface in the SRO phase. Application of GGA to magnetism should be taken with caution since it does not correctly account for correlations, but given the proximity to Stoner instability, it is possible that the interface is in or energetically very close to a ferromagnetic ground state.

Our study provides a possible explanation of the enhancement of the superconducting T_C when Ru metal inclusions are present. We find that these inclusions form microscopically well-ordered interfaces and structure. The interfaces acts as "ladder" which couple the superconducting order parameter of a large number of RuO_2 SRO layers over a micrometer-size length. These inclusions should lead to an interlayer coupling which can significantly reduce the superconducting order parameter phase fluctuations, thereby increasing the superconducting critical temperature.

This observation opens up exciting prospects when a similar growth process is applied to the case of the cuprate superconductors. If these inclusions introduce an interlayer Josephson-Junction type coupling, we should expect a significant enhancement of the superconducting critical temperature.

VI. ACKNOWLEDGMENTS

This work was supported in part by the U.S. National High Magnetic Field Laboratory, which is partially funded by the NSF DMR-1157490 and the State of Florida.

[1] A. P. Mackenzie and Y. Maeno, Rev. Mod. Phys. **75**, 657 (2003).
[2] Y. Maeno, H. Hashimoto, K. Yoshida, S. Nishizaki, T. Fujita, J. G. Bednorz, and F. Lichtenberg, Nature **372**, 532 (1994).
[3] Y. Maeno, S. Kittaka, T. Nomura, S. Yonezawa, and K. Ishida, Journal of the Physical Society of Japan **81**, 011009 (2012).
[4] K. Ishida, Y. Kitaoka, K. Asayama, S. Ikeda, S. Nishizaki, Y. Maeno, K. Yoshida, and T. Fujita, Phys. Rev. B **56**, R505 (1997).
[5] K. Ishida, H. Mukuda, Y. Kitaoka, K. Asayama, Z. Q. Mao, Y. Mori, and Y. Maeno, Nature **396**, 658 (1998).
[6] S. Nishizaki, Y. Maeno, S. Farner, S. ichi Ikeda, and T. Fujita, Journal of the Physical Society of Japan **67**, 560 (1998).
[7] K. D. Nelson, Z. Q. Mao, Y. Maeno, and Y. Liu, Science **306**, 1151 (2004).
[8] J. Jang, D. G. Ferguson, V. Vakaryuk, R. Budakian, S. B. Chung, P. M. Goldbart, and Y. Maeno, Science **331**, 186 (2011).
[9] G. M. Luke, Y. Fudamoto, K. M. Kojima, M. I. Larkin, J. Merrin, B. Nachumi, Y. J. Uemura, Y. Maeno, Z. Q. Mao, Y. Mori, H. Nakamura, and M. Sigrist, Nature **394**, 558 (1998).
[10] J. Xia, Y. Maeno, P. T. Beyersdorf, M. M. Fejer, and A. Kapitulnik, Phys. Rev. Lett. **97**, 167002 (2006).
[11] I. I. Mazin and D. J. Singh, Phys. Rev. Lett. **79**, 733 (1997).
[12] T. M. Rice and M. Sigrist, Journal of Physics: Condensed Matter **7**, L643 (1995).
[13] G. Baskaran, Physica B: Condensed Matter **223**, 490 (1996).
[14] A. P. Mackenzie, S. R. Julian, A. J. Diver, G. J. McMullan, M. P. Ray, G. G. Lonzarich, Y. Maeno, S. Nishizaki, and T. Fujita, Phys. Rev. Lett. **76**, 3786 (1996).
[15] T. Oguchi, Phys. Rev. B **51**, 1385 (1995).

[16] D. J. Singh, Phys. Rev. B **52**, 1358 (1995).
[17] P. K. de Boer and R. A. de Groot, Phys. Rev. B **59**, 9894 (1999).
[18] X.-P. Hao, H.-L. Cui, Z.-L. Lv, and G.-F. Ji, Physica B: Condensed Matter **441**, 62 (2014).
[19] Y. Sidis, M. Braden, P. Bourges, B. Hennion, S. NishiZaki, Y. Maeno, and Y. Mori, Phys. Rev. Lett. **83**, 3320 (1999).
[20] S. V. Halilov, D. J. Singh, J. Minár, A. Y. Perlov, and H. Ebert, Phys. Rev. B **71**, 100503 (2005).
[21] I. I. Mazin and D. J. Singh, Phys. Rev. Lett. **82**, 4324 (1999).
[22] S. Kittaka, H. Taniguchi, S. Yonezawa, H. Yaguchi, and Y. Maeno, Phys. Rev. B **81**, 180510 (2010).
[23] C. W. Hicks, D. O. Brodsky, E. A. Yelland, A. S. Gibbs, J. A. N. Bruin, M. E. Barber, S. D. Edkins, K. Nishimura, S. Yonezawa, Y. Maeno, and A. P. Mackenzie, Science **344**, 283 (2014).
[24] Y. A. Ying, N. E. Staley, Y. Xin, K. Sun, X. Cai, D. Fobes, T. J. Liu, Z. Q. Mao, and Y. Liu, Nature Communications **4**, 2596 EP (2013), article.
[25] H. Wang, W. Lou, J. Luo, J. Wei, Y. Liu, J. E. Ortmann, and Z. Q. Mao, Phys. Rev. B **91**, 184514 (2015).
[26] Y. Maeno, T. Ando, Y. Mori, E. Ohmichi, S. Ikeda, S. NishiZaki, and S. Nakatsuji, Phys. Rev. Lett. **81**, 3765 (1998).
[27] Z. Q. Mao, K. D. Nelson, R. Jin, Y. Liu, and Y. Maeno, Phys. Rev. Lett. **87**, 037003 (2001).
[28] T. Ando, T. Akima, Y. Mori, and Y. Maeno, Journal of the Physical Society of Japan **68**, 1651 (1999).
[29] M. Sigrist and H. Monien, Journal of the Physical Society of Japan **70**, 2409 (2001).
[30] Y. A. Ying, Y. Xin, B. W. Clouser, E. Hao, N. E. Staley, R. J. Myers, L. F. Allard, D. Fobes, T. Liu, Z. Q. Mao, and Y. Liu, Phys. Rev. Lett. **103**, 247004 (2009).
[31] Y. Maeno, T. M. Rice, and M. Sigrist, Physics Today **54**, 42 (2001).
[32] P. E. Blöchl, Phys. Rev. B **50**, 17953 (1994).
[33] M. Shishkin, M. Marsman, and G. Kresse, Phys. Rev. Lett. **99**, 246403 (2007).
[34] F. Fuchs, J. Furthmüller, F. Bechstedt, M. Shishkin, and G. Kresse, Phys. Rev. B **76**, 115109 (2007).
[35] M. Shishkin and G. Kresse, Phys. Rev. B **75**, 235102 (2007).
[36] M. Shishkin and G. Kresse, Phys. Rev. B **74**, 035101 (2006).
[37] J. P. Perdew, K. Burke, and M. Ernzerhof, Phys. Rev. Lett. **77**, 3865 (1996).
[38] X. Wan, A. M. Turner, A. Vishwanath, and S. Y. Savrasov, Phys. Rev. B **83**, 205101 (2011).
[39] R. Matzdorf, Z. Fang, Ismail, J. Zhang, and e. al, Science **289**, 746 (2000), copyright - Copyright American Association for the Advancement of Science Aug 4, 2000; Last updated - 2010-06-08; CODEN - SCIEAS.
[40] W. Tang, E. Sanville, and G. Henkelman, Journal of Physics: Condensed Matter **21**, 084204 (2009).
[41] N. Pavlenko, T. Kopp, E. Y. Tsymbal, J. Mannhart, and G. A. Sawatzky, Phys. Rev. B **86**, 064431 (2012).
[42] E. W. Carlson, S. A. Kivelson, V. J. Emery, and E. Manousakis, Phys. Rev. Lett. **83**, 612 (1999).

Appendix A: Partial DOS

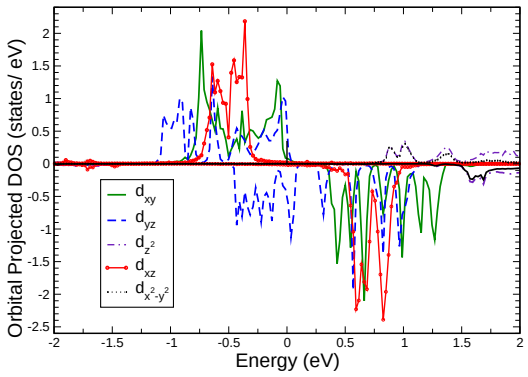

FIG. 8. Y_{lm}-projected density of states for a Ru atom in the SRO phase. The e_g orbitals are unoccupied and and pushed away from the t_{2g} orbitals due to the crystal field. The magnetic moments ($M_{Ru} = 1.532\,\mu_B$) are a result of the t_{2g} spin-split. Spin-up is above the horizontal axis and spin-down below the axis. The Fermi level is at zero.

In contrast to a ruthenium atom of the interface column, the Ru atoms in the SRO phase are located at the center of an oxygen octahedra. Due to crystal field symmetry, they have a clear t_{2g}-e_g split, as can be seen in Fig. 8. The t_{2g} orbitals are clearly spin split, causing the significant magnetic moments discussed in the main text. This picture is in contrast to the $SrTiO_3/LaAlO_3$ interface[41], where an e_g splitting is associated with magnetic order.

Fig. 9 shows the partial density of states of an oxygen atom bonded to one of the interface column ruthenium atoms showing a Fermi level contribution of all three p-orbitals. The orbital character is determined by the unique

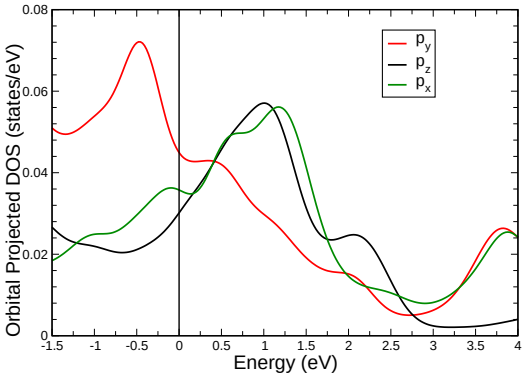

FIG. 9. Y_{lm}-projected density of states for a oxygen atom bonded to an interface Ru. The Fermi level (placed at zero) is is occupied by all three p-orbitals. A Lorentzian smear of 0.2 eV has been applied to the dos data.

coordination number of the Ru atoms at the interface and makes is marked by an absence of octahedral symmetry and enhanced hybridization.